



HAL
open science

Fabrication and Packaging of Flexible Polymeric Microantennae for in Vivo Magnetic Resonance Imaging

Magdalèna Couty, Marion Woytasik, Jean-Christophe Ginefri, Anne Rubin, Emile Martincic, Marie Poirier-Quinot, Luc Darrasse, Fawzi Boumezbeur, Franck Lethimonnier, Michael Tatoulian, et al.

► To cite this version:

Magdalèna Couty, Marion Woytasik, Jean-Christophe Ginefri, Anne Rubin, Emile Martincic, et al.. Fabrication and Packaging of Flexible Polymeric Microantennae for in Vivo Magnetic Resonance Imaging. *Polymers*, 2012, 4 (1), pp.656-673. 10.3390/polym4010656 . hal-02270008

HAL Id: hal-02270008

<https://hal.science/hal-02270008>

Submitted on 23 Aug 2019

HAL is a multi-disciplinary open access archive for the deposit and dissemination of scientific research documents, whether they are published or not. The documents may come from teaching and research institutions in France or abroad, or from public or private research centers.

L'archive ouverte pluridisciplinaire **HAL**, est destinée au dépôt et à la diffusion de documents scientifiques de niveau recherche, publiés ou non, émanant des établissements d'enseignement et de recherche français ou étrangers, des laboratoires publics ou privés.

Article

Fabrication and Packaging of Flexible Polymeric Microantennae for *in Vivo* Magnetic Resonance Imaging

Magdalèna Couty^{1,2,3}, Marion Woytasik^{1,2}, Jean-Christophe Ginefri^{2,4}, Anne Rubin^{1,2,5}, Emile Martincic^{1,2}, Marie Poirier-Quinot^{2,4}, Luc Darrasse^{2,4}, Fawzi Boumezbeur⁵, Franck Lethimonnier⁵, Michael Tatoulian³ and Elisabeth Dufour-Gergam^{1,2,*}

¹ Univ. Paris Sud, Laboratoire IEF (Institut d'Electronique Fondamentale), UMR-8622, Bat. 220, F-91405 Orsay, France; E-Mails: magdalena.couty@u-psud.fr (M.C.); marion.woytasik@u-psud.fr (M.W.); emile.martincic@u-psud.fr (E.M.);

² CNRS (Centre National de Recherche Scientifique), F-91405 Orsay, France; E-Mails: jean-christophe.ginefri@u-psud.fr (J.-C.G.); anne.rubin@ics-cnrs.unistra.fr (A.R.); marie.poirier-quinot@u-psud.fr (M.P.-Q.); luc.darrasse@u-psud.fr (L.D.)

³ LGPPTS (Laboratoire du Génie des Procédés Plasmas et Traitements de Surface), Chimie ParisTech/UPMC EA3492, 11 rue Pierre et Marie Curie, F-75005 Paris, France; E-Mail: michael-tatoulian@chimie-paristech.fr (M.T.)

⁴ Univ. Paris Sud, Laboratoire IR4M (Imagerie par Résonance Magnétique Médicale et Multi-Modalités), UMR-8081, Bat. 220, F-91405, Orsay, France

⁵ I2BM (Institut d'Imagerie BioMédicale), Neurospin, CEA Saclay, Bat. 145, F-91191 Gif-sur-Yvette, France; E-Mails: fawzi.boumezbeur@cea.fr (F.B.); franck.lethimonnier@cea.fr (F.L.)

* Author to whom correspondence should be addressed; E-Mail: elisabeth.dufour-gergam@u-psud.fr; Tel.: +33-169-157-723; Fax: +33-169-154-080.

Received: 23 December 2011; in revised form: 14 January 2012 / Accepted: 15 February 2012 / Published: 27 February 2012

Abstract: In this paper, we detail how microantennae dedicated to Magnetic Resonance Imaging (MRI) can benefit from the advantages offered by polymer substrates, especially flexibility and dielectric properties. We present a monolithic and wireless design based on the transmission lines between conductor windings on both sides of a dielectric substrate and its fabrication process. This last one requires specific plasma treatments to improve polymer/metal adhesion. We have led a comparative study on the effects of the ageing time on the wettability and the metal adhesion to Kapton and Teflon surfaces. Correlation

between wettability (water contact angle) and adhesion (tensile strength) has been established. Then, the use of PolyDiMethylSiloxane (PDMS) as biocompatible packaging material and the optimization of its thickness allows us to conserve suitable f_0 and Q values in a conducting environment such as the biological tissues. These studies allow us to perform 7 Tesla *in vivo* MRI of the rat brain with a high spatial resolution of $100 \times 100 \times 200 \mu\text{m}^3$ and a Signal to Noise Ratio of 80.

Keywords: MRI; flexible microantenna; plasma treatment; PDMS

1. Introduction

The use of polymers in the microsystem field has spread these last years. Indeed, they are low-cost while allowing batch fabrication by microtechnologies. Contrary to the substrates traditionally used in the field, such as silicon or silicone oxide, they offer high flexibility and a wide range of dielectric properties for numerous applications, e.g., stretchable electronics and implantable medical devices. In the case of implantable microdevices, flexibility is especially desirable to reduce the damage inflicted during surgery and for the comfort of the patient during the implantation [1]. Moreover, polymers also have interesting interactions with the biological tissues: the biocompatible ones as packaging materials and the biodegradable ones for drug delivery.

We develop microantennae on polymer substrates for Magnetic Resonance Imaging (MRI) on the microscopic scale so we have considered how this kind of devices can benefit from the advantages described above. Our approach consists in reducing the size of the antenna to increase its sensitivity and therefore to obtain higher Signal to Noise Ratio (SNR). This approach has been already validated for the classic configuration of macroscopic antennas [2,3]. Miniaturization of macroscopic MRI antennas is limited to the centimeter scale by the use of discrete components such as tuning and matching capacitors [3,4]. To overcome this limitation, a solution is to use a monolithic design based on transmission lines. We have developed a monolithic design based on the transmission lines between conductor windings on both sides of a dielectric substrate, called Multi-turn Transmission Lines Resonator (MTLR) [5]. Coils with similar designs (also based on transmission lines) have been fabricated on various rigid substrates such as silicon dioxide [6] and glass [7], then on flexible polymeric substrates such as polyimide [7–9] and Teflon [10,11]. This last substrate has a low loss tangent (less than 0.0003 at 1 MHz) which allows to reduce the parasitic capacitance and maximize the quality factor Q of the antennas [11].

In the case of surface imaging, flexible antennas conform very close to curved surfaces and provide improved images, compared with planar antennas [12]. A concern about flexibility could be the performances of the antennas when they are bent. For surface imaging, the bending is relatively low and no significant variation of the resonant frequency f_0 and the quality factor Q is observed. However, other applications need a stronger bending such as catheter tracking by MRI. Ahmad *et al.* reported that wrapping flexible antennas fabricated on polyimide and SU-8 substrates round the catheter alters their inductances thus shifts f_0 and subsequent tuning and matching are necessary [13]. Ellersiek *et al.* studied the influence of the bending radius on the inductance of the antenna and determined that it

decreases to 20% when this radius is very low [14]. Microfabricated catheter-mounted coils are now reasonably developed, and can be bent without significantly degrading their performance [15]. Moreover, this specific application remains the most extreme case of bending conditions for MRI antennas.

When imaging tissues deeply inside the body is required, as microantennae have a limited field of view, they must be implanted [3]. In this case, MRI becomes invasive but offers the possibility of an easy long-term monitoring. Besides flexibility, additional specifications for the design and the packaging have to be defined to reduce as much as possible the invasive aspect of implantation. The antenna should be very small (*i.e.*, about a few millimeters) and without wire connection. Our MTLR design is totally in agreement with these specifications. Furthermore, packaging the antenna with an adequate biocompatible polymer minimizes its impact on the surrounding environment. Reciprocally, the antenna must be protected from the undesirable effects of the biological tissues on its characteristics. Indeed, they have a high permittivity (about 80) and a high conductivity (about 0.7 S/m) thus induce by dielectric coupling a shift-down of f_0 and degradation of Q . This phenomenon has been observed by Yung *et al.* and Bilgen [3,4]. Dielectric and biocompatibility properties of polymers make them also appropriate as packaging materials for implanted MRI microantennae. Bilgen chose to apply a thick biocompatible elastomer coating to increase the distance between the antenna and the tissues and so to reduce the coupling effect [4]. We chose to work with PolyDiMethylSiloxane (PDMS), the most common silicone elastomer, which is widely considered as biocompatible for short-term (days) implantation [16] and has a low permittivity (2.65 at 100 kHz) and a low loss tangent (1×10^{-3} at 100 kHz). Its preparation and deposition need no specific expensive equipment and an accurate control of thickness can be achieved through spin coating parameters (rotation speed, time) and curing conditions (temperature, time). Moreover, thickness of several hundred micrometers may be deposited, which is not possible with other biocompatible coating materials such as parylene.

Despite the numerous advantages of polymers explained above, their main drawback is the poor adhesion of metal to their surface. Surface modifications by plasma treatments are the most common solution to overcome this drawback. Each polymer requires a specific plasma treatment depending on its chemistry. The efficiency of oxygen plasma exposure for polyimide is well-known [17]. In a previous work [12], we used this method to fabricate flexible microantennae (with MTLR design) on Kapton and showed how they improve the *in vivo* surface imaging at 2.35 Tesla of a subcutaneous tumor in mouse by form-fitting to the skin.

However, fluorinated polymers are very hydrophobic [18] and a reliable adhesion of metal to their surfaces is difficult to obtain. Zhang *et al.* fabricated large-sized antennas (about 10×10 cm² squares) with copper tape on Teflon films [10], whereas Eroglu *et al.* directly used commercial metalized films [11]. Studies were necessary to find an efficient plasma treatment to improve the metal adhesion to the Teflon surface. These studies led to a low pressure N₂/H₂ plasma [19] and have allowed us to fabricate flexible microantennae (still with MTLR design) on Teflon substrates. The project aims to use MRI as a diagnosis and monitoring tool for tumors and neurodegenerative diseases, *i.e.*, Alzheimer's one, in clinical research on small rodents, and has evolved to 7 Tesla *in vivo* imaging of the rat brain using implanted microantennae. In this paper, after description of the MTLR design and its fabrication process, we present a comparative study on the improvement of polymer/metal adhesion by specific plasma treatments on Kapton and Teflon films, the optimization of the PDMS packaging to

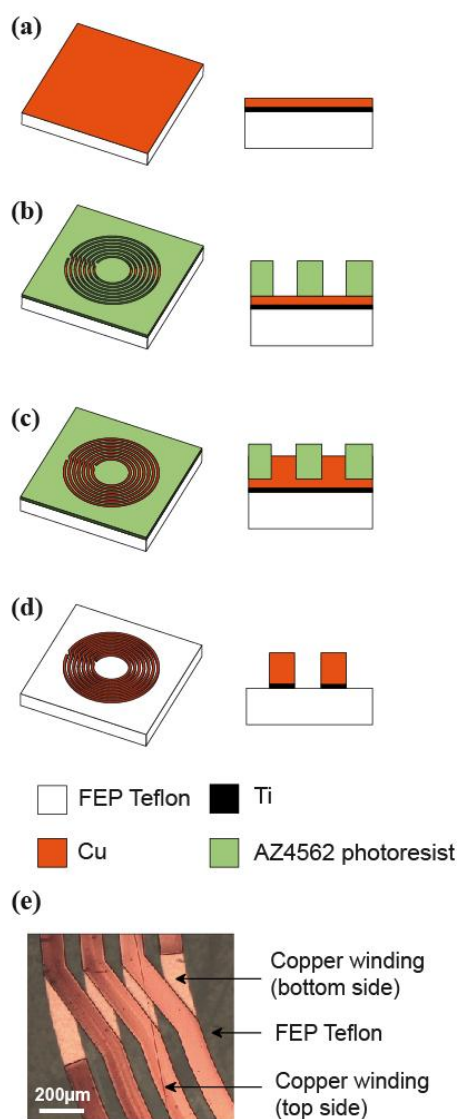
conserve the desired electrical characteristics in a conducting environment and finally *in vivo* imaging of the rat brain.

2. Experimental Section

2.1. Fabrication Process

The substrates are polyimide 125 μm -thick Kapton HN films from DuPont Nemours® and FEP Teflon films from MICEL®. The antennas are fabricated on these flexible polymer substrates using the copper micromoulding process detailed in [7,20]. Figure 1 summarizes the different steps of the process.

Figure 1. Steps of copper micromoulding process: **(a)** Ti/Cu:10/100 nm sputtering, **(b)** patterning 20 μm AZ4562 photoresist mould by photolithography, **(c)** 10 μm copper electrodeposition, **(d)** photoresist removal and wet etching of seed layer; **(e)** view of the alignment between the copper windings on the top and the bottom sides by transparency through the Teflon substrate.



First, a metallic seed layer Ti/Cu:10/100 nm is deposited by sputtering on the polymer film (a). The metalized film is glued with photoresist on a rigid glass support to ensure a flat surface and the rigidity of the sample for the subsequent steps. The 20 μm -thick AZ4562 mould is patterned by photolithography (b). The patterned mould is filled with 10 μm copper by electrodeposition (c). This thickness allows avoidance of the increase of the series resistance due to the skin effect—skin depth is 3.77 μm at 300 MHz for copper. Finally, the photoresist is removed by acetone and the seed layer is removed by wet etching (d). These steps are repeated for the second side of the substrate, with an accurate alignment of the windings by transparency through glass using a EVG®620 double-side lithography equipment (e).

2.2. Plasma Treatments

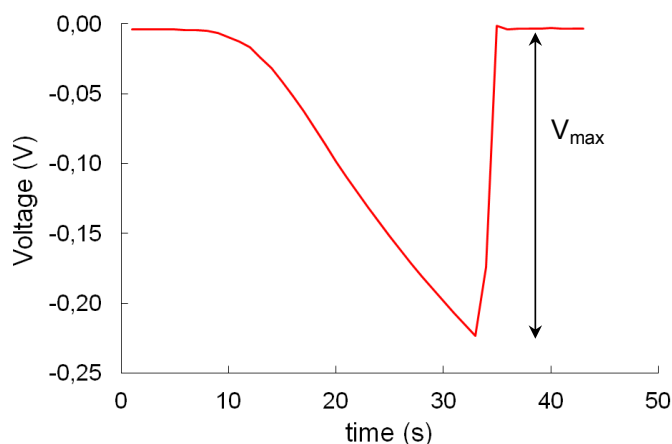
The Kapton films are treated with an O_2 plasma in a plasma etcher Pico UHP from Diener electronic. The O_2 pressure is adjusted to 0.6 mbar and the plasma is produced using a 40 kHz RF generator with a power of 120 W, during a treatment time of 90 s.

The treatment of the FEP Teflon films is performed in a low pressure home-made plasma reactor with an asymmetric electrode configuration described in [21]. The rotary cylindrical grounded electrode and the high-voltage knife electrode are spaced of 8 mm. The cylinder—length 22 cm, diameter 7 cm—is also a carrier for the samples and is protected by a polyethylene film. A base pressure of 3×10^{-2} mbar is reached using a turbo molecular pumping system and a chemical pump. Then, the gaseous mixture N_2/H_2 :25/75% (v/v) is introduced and the pressure is adjusted to 0.600 mbar. The plasma is produced between the two electrodes. A Corona discharge is provided by a 70 kHz RF generator with a power of 2 W for an effective treatment time of 5 s.

2.3. Tensile Strength Measurements by Pull-Off System

The tensile strength is measured for both untreated and plasma treated Kapton and Teflon samples about 1 cm^2 . A Ti/Cu seed layer has been deposited by sputtering on all these samples (few hours or days after the plasma exposure for treated samples). Measurements of tensile strength are performed using a home-made pull-off set-up similar to described in [22,23]. The samples are prepared using the following method: the bottom side of the metalized polymer film is glued with epoxy on a brass carrier. A metal stud, 4 mm in diameter, is glued on the center of the metallic surface. After one hour in oven at 60 $^\circ\text{C}$ to ensure a reproducible curing of the epoxy glue, and a slow cooling to room temperature, the sample is mechanically held in the pull-off system. The pulling force is progressively applied by pumping. The voltage detected by the force sensor is amplified and measured with a numerical multimeter. The calibration of the system, for each amplification range, allows us to deduce the tensile strength from the maximal variation of the voltage (V_{max}) measured at the breaking point. Figure 2 shows the typical acquisition curve using this system.

Figure 2. Typical acquisition curve of the voltage with time, from the pull-off system.



2.4. Electromagnetic Characterization of the Antennas

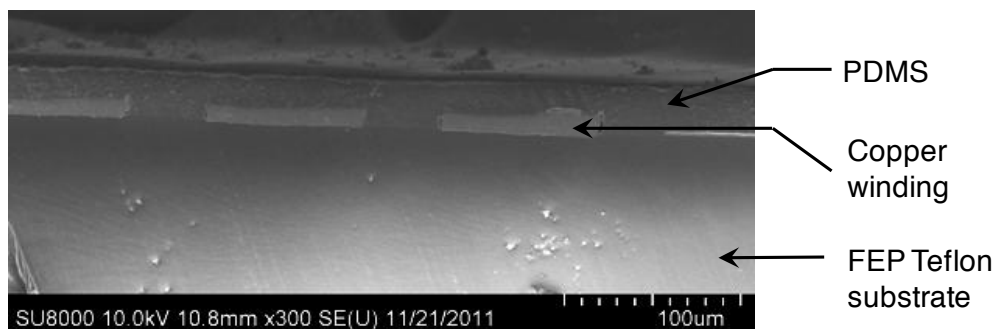
To limit the cross effect between neighboring antennas, the batch substrate is cut to obtain single antenna which will be individually characterized. The resonant frequency f_0 and the quality factor Q are measured using the single-loop probe method [24] and a E5061A network analyzer from Agilent Technologies. The magnetic coupling between the antenna and the single loop must be sufficiently weak so that the performances of the antenna are not affected by the presence of the probe and are neither dependent on the input nor on the distance between the probe and the antenna. This condition is achieved when the reflection coefficient at the single loop terminal is less than -40 dB [25].

Saline agar phantoms are prepared with 5% agarose gel in NaCl 0,45% Cooper® solution. Permittivity is about 80 and electrical conductivity about 0.7 S/m, close to the electrical properties of biological tissues in the rat brain. Measurements are performed in air and in agar phantom to evaluate the influence of a conducting environment on the performances of the antenna.

2.5. PDMS Packaging

PDMS is prepared using the commercial kit Sylgard184® provided by Dow Corning. The silicone polymer and the curing are mixed in a 10:1 weight ratio and then placed under vacuum for one hour to remove all bubbles. To improve the adhesion of PDMS on the antenna, its surface is treated with a He/O₂:50/50% (v/v) plasma [26,27] in the low pressure reactor described in Section 2.2. The power and pressure conditions are similar to the ones used for the N₂/H₂ treatment. In this case, the surface modifications are more stable because helium species participate to crosslink the upper-most surface layer, minimizing side chain reorganization [28]. Then, the PDMS mixture is deposited by spin-coating to ensure accurate control of the thickness through the parameters (speed rotation, time). The PDMS is cured at 95 °C for 30 min in an oven. Under these conditions, the resulting thickness is about 30 μm. This process is repeated for each side of the antenna. To observe the deposition profile of PDMS on the copper windings, an antenna is fractured after cryopreparation. Figure 3 shows a SEM view of the cross section. The gap between the windings is completely filled with PDMS and the surface of the deposit is flat. Note that the difference in the thermal expansion coefficient of the materials may provoke small localized gaps at the copper/PDMS interface.

Figure 3. SEM view of the cross section of the PolyDiMethylSiloxane (PDMS) layer deposited on a Teflon antenna.

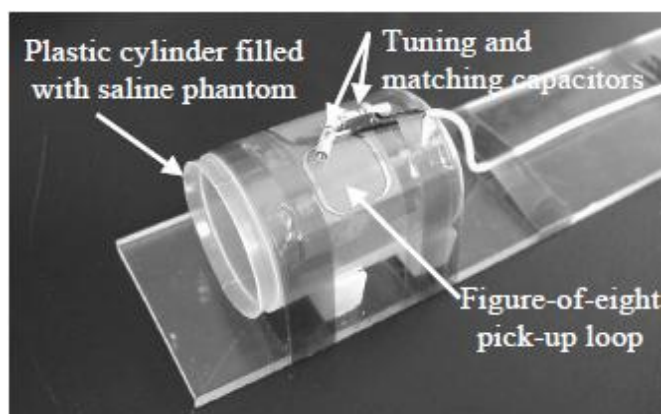


To investigate the impact of the PDMS thickness on the characteristics of the antenna, the thickness is progressively increased, with a path of 20 μm , and measurements of f_0 and Q factor are systematically made after each increment. The study is led on 3 groups of 2 or 3 exactly identical antennas. Good reproducibility is observed in each group. The size of the antenna (less than 1 cm^2) is too small to keep uniform deposition with successive PDMS layers deposited by spin-coating. Therefore, 20 μm -thick PDMS films are separately prepared on a FEP Teflon substrate which has not received any plasma treatment and thus has a low surface energy. Adhesion of these films to the FEP surface is very poor and so they may be easily transferred to the surface of the antenna. A surface activation by O_2 plasma (pressure 0.4 mbar, power 240 W, time 90 s in the etcher Pico UHP) between two increments is required.

2.6. Magnetic Resonance Imaging

MRI experiments are performed in Neurospin platform in CEA Saclay on a 7 Tesla horizontal bore magnet (Pharmascan, Brüker Biospin, Ettlingen, Germany) driven by a Paravision 5.1 console (Brüker, Ettlingen Germany) and equipped with a 720 mT/m actively shielded gradient device (100 μs rise time). The NMR signal is transferred from the implanted coil to the receiver channel of the MRI unit by inductive coupling via an external pick-up loop (Figure 4).

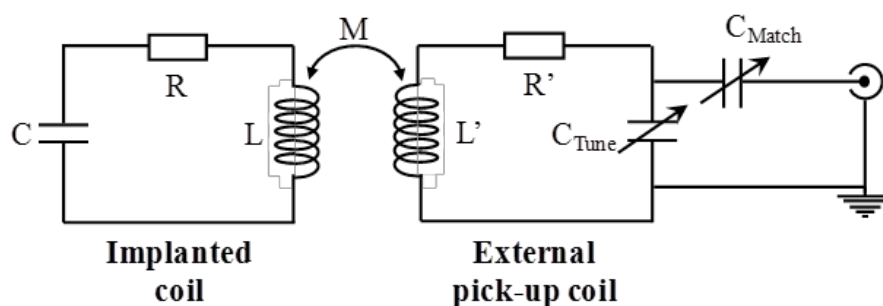
Figure 4. Experimental set-up of the figure-of-eight pick-up loop and the gel phantom for MRI.



The pick-up loop is based on the figure-of-eight design. It consists of two loops connected in series with opposite current flow direction, thus producing a magnetic field perpendicular to the pick-up loop plane. The external pick up loop is tuned using a non magnetic trimmer capacitor (0.8–8 pF) connected in at the pick-up loop terminal. Impedance matching to the 50 Ω input of the receiver channel is achieved by adjusting a non magnetic trimmer capacitor (0.8–8 pF) connected in series in between the tuning capacitor and the copper core of the coaxial cable.

The equivalent electrical circuit of the implanted coil inductively coupled to the external pick-up loop is shown in Figure 5. In practice, the mutual inductance between the implanted coil and the external pick-up loop is fixed. Tuning and matching are performed by iterative adjustments of the capacitors values and typical matching level of -30 dB are achieved. For phantom imaging, the pick-up loop is fixed on a plastic cylinder which contains the agar gel.

Figure 5. Equivalent electrical circuit of the implanted coil inductively coupled to the external pick-up coil. C_{Tune} and C_{Match} are the tuning capacitor and the matching capacitor, respectively, and consisted of (0.8-8 pF) non magnetic trimmer capacitor.

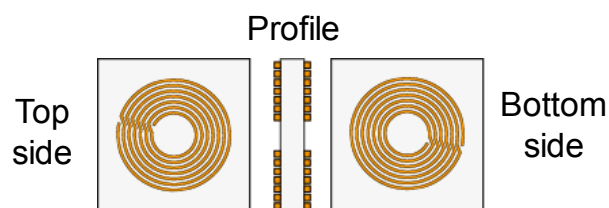


All *in vivo* experiments are conducted according to EEC guidelines and directives (86/09/EEC). An adult male Sprague-Dawley rat (300 g) is deeply anaesthetized with ketamine/xylazine (50/7.5 mg kg⁻¹, i.p.). The anaesthetized rat is immobilized in a stereotaxic apparatus. After sterilization, the microantenna is surgically implanted at the level of the interhemispheric cleft close to the cingulate cortices. The scalp is sutured before placing the anaesthetized animal inside a cradle apparatus. Animal respiration and temperature are monitored. Upon completion of the *in vivo* MRI experiments, the animal is euthanized and the antenna is retrieved.

3. Results and Discussion

3.1. Multi-Turn Transmission Line Resonator Design

Multi-turn Transmission Line Resonator (MTLR) design [5] consists in conductor (copper) lines—concentric split-rings connected in series—deposited on both sides of a dielectric substrate (polymer film) as shown in Figure 6. The MTLR structures are self-resonant and achieve both the RF field emission for nuclear magnetic excitation with amplification, and then the amplification and detection of the resulting NMR signal without the need of any wire connection.

Figure 6. Multi-turn transmission line resonator.

MRI requires that the f_0 of the antenna match the Larmor frequency ν_0 , given in Equation (1):

$$\nu_0 = \frac{\gamma}{2\pi} B_0 \quad (1)$$

where B_0 is the static magnetic field and γ is the gyromagnetic ratio of the nucleus. The nucleus is generally the proton ^1H for its abundance in the tissues (mainly composed of water) and its high sensitivity (γ of 42.576 MHz/Tesla). The Larmor frequency for ^1H with $B_0 = 7$ Tesla is 299 MHz. An analytical model has been developed for the MTLR design to define the geometrics parameters of the antennas, depending on the dielectric properties of the substrate and its thickness, to target a given f_0 . The full description of the multi-turn transmission line design, including the behavioral analysis of the resonance condition and the formulae used for equivalent transmission line parameters determination can be found in [29]. We expect a decrease of f_0 value with the packaging, according to the permittivity value of PDMS, thus we target a wide f_0 range from 300 to 400 MHz. The geometric parameters are given in Table 1 for this frequency range and Fluorinated Ethylene Propylene (FEP), a variety of Teflon, as substrate. These micrometric dimensions imply to use microfabrication technologies in a clean room.

Table 1. Geometric parameters of the antennas defined for 7 Tesla MRI.

Diameter (mm)	Number of turns	Width of the winding (μm)	Gap between two windings (μm)
5.4 to 6.0	6	88	40

3.2. Improvement of Polymer/Metal Adhesion by Plasma Treatment

The microantennae are fabricated using the copper micromoulding process described in the Experimental Section. The first step of this process is the deposition of a metallic seed layer by sputtering on the polymer film. As previously detailed, because of the low adhesion of metal to polymer surfaces, specific plasma treatments before metallization are needed. The efficiency of the plasma treatments have been assessed by measuring the Water Contact Angle (WCA) and adhesion properties with tensile strength measurements, for both untreated and treated samples. The study is led on FEP Teflon, our substrate of interest, and on Kapton which is widely used and well-known in our team. Kapton films are treated using O_2 plasma exposure in a reactor placed in the same clean room than the sputtering equipment, allowing the immediate subsequent metallization. The N_2/H_2 specific plasma treatment for Teflon is carried out in another laboratory that implies an incompressible ageing time of 3 h for the surface modifications before metallization. During the transportation, the samples

are kept under vacuum to limit the evolution of surface modifications, *i.e.*, adsorption of atmospheric contaminants and short range reorganization of side chains. For this reason, we have studied the influence of the ageing time on the wettability of the surface and on the polymer/metal adhesion for Kapton and Teflon films.

Hydrophilic surfaces are considered to be more suitable to obtain a good adhesion. Figures 7 and 8 show the WCA before and immediately after the plasma exposure for Kapton and Teflon films. In both cases, the WCA is decreased by the plasma treatment. For Kapton, it decreases from 72° to 10° , resulting in a highly hydrophilic surface which should provide a stronger adhesion of metal. For Teflon, the surface is very hydrophobic before the treatment (WCA of 107°). After treatment, the WCA is decreased to 63° which makes the film more likely to ensure a reliable adhesion of metal. The variation induced by the plasma exposure is due to the creation of polar groups on the surface which increases its wettability. In the case of Kapton in oxygen atmosphere, the amount of oxygenated moieties increases, while for Teflon in N_2/H_2 atmosphere fluorine atoms are removed by H radicals and replaced by amino moieties. Detailed characterization of the surface modifications by X-Ray Photoelectron Spectroscopy (for chemical aspects) and Atomic Force Microscopy (for topography aspects) are currently in progress.

Figure 7. Water Contact Angle (WCA) before (a) and after (b) plasma treatment for a Kapton film.

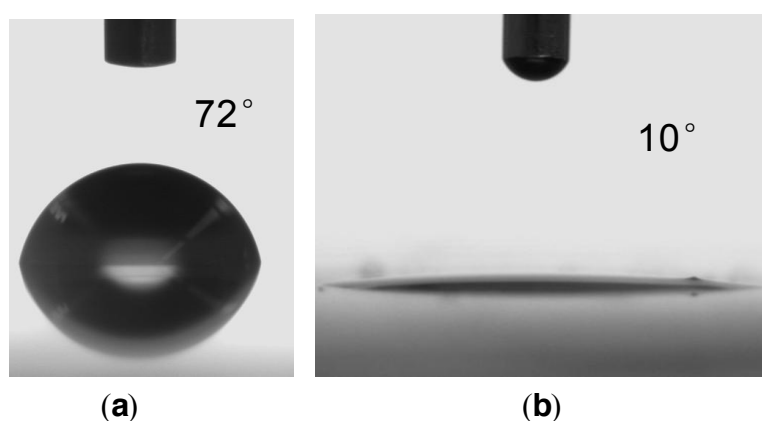
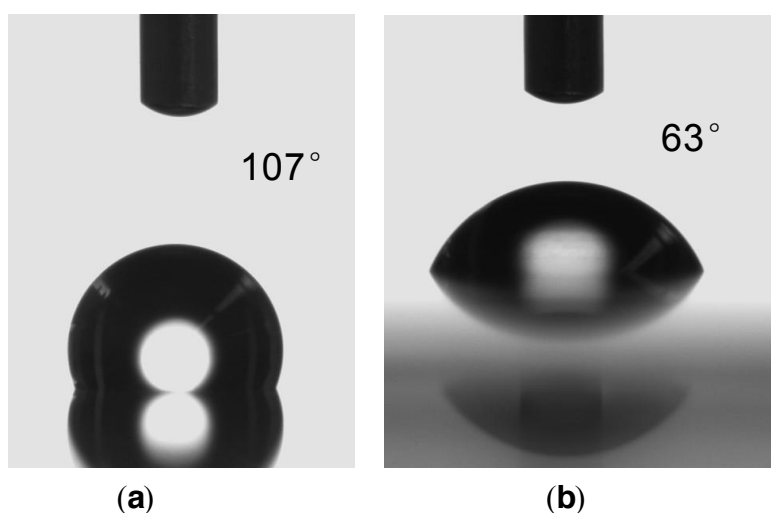


Figure 8. WCA before (a) and after (b) plasma treatment for a FEP Teflon film.



The evolution of these surface modifications is evaluated by WCA measurements for several days after the treatment (Figure 9). Measurements are also performed on untreated samples as a reference. Both Kapton and Teflon untreated samples show only a negligible variation around the initial value. However, the WCA of treated samples increases with time, especially in the first hours after the plasma exposure. After the first hours, the increase is slower, probably corresponding to the stabilization of the surface modifications. It reaches a value of 27° for Kapton after 7 days while the value for Teflon after 5 days is 76° . The WCA variation may be explained by rearrangement within the modified layer, that is through short-range reorientation of side chains [28] (Figure 10). In all cases, even several days after the treatment, the WCA for treated sample is still lower than that obtained for the untreated sample. The WCA is also still lower for Kapton than Teflon samples, both treated and untreated.

Figure 9. Evolution of WCA with time for untreated and treated Kapton and FEP Teflon films.

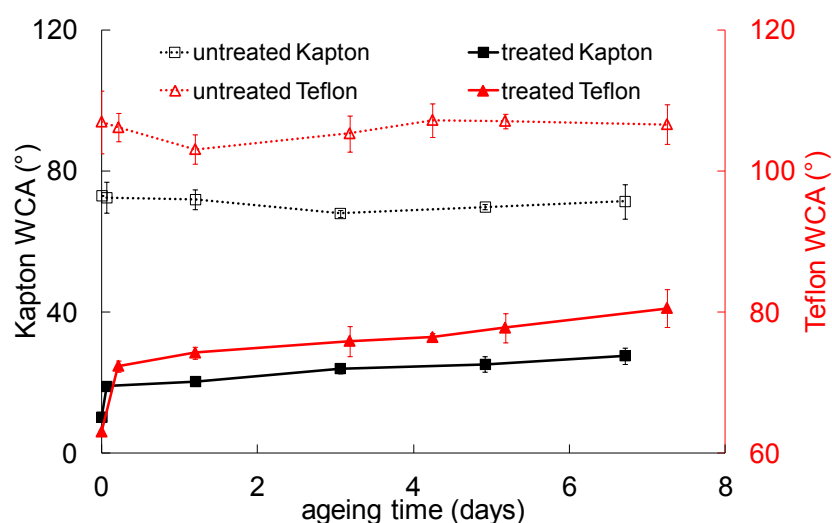
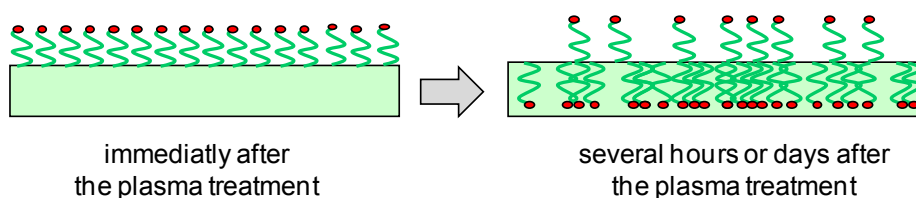


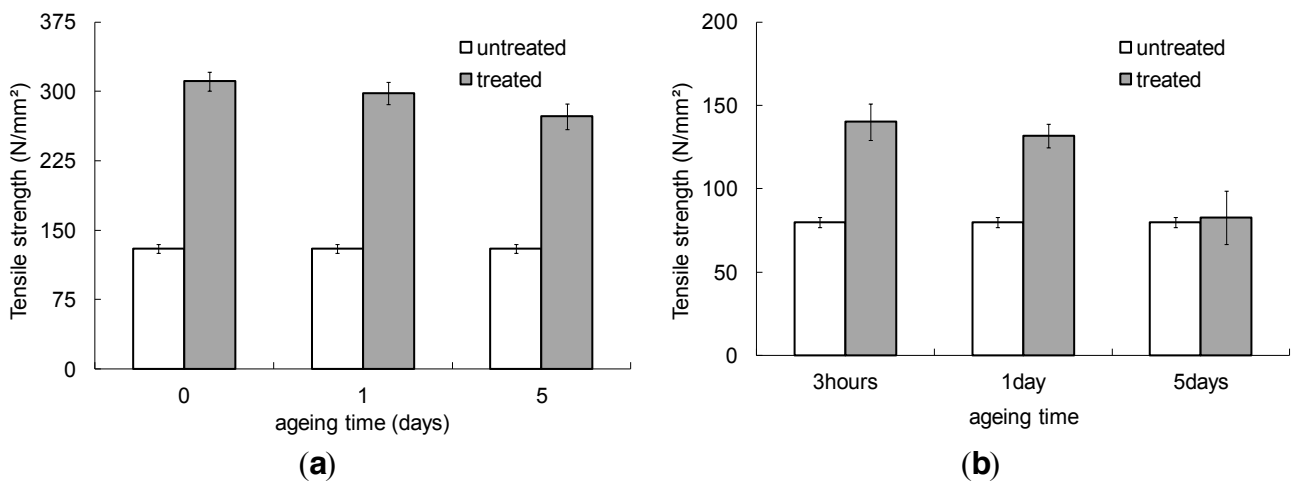
Figure 10. Scheme explaining ageing phenomenon due to short range reorientation of side chains.



To establish a correlation between the WCA and the polymer/metal adhesion, a thin metallic layer is deposited on the treated films after different ageing times: the shortest, *i.e.*, 3 h for Teflon and quasi immediately for Kapton, then 1 day and 5 days. Figure 11 shows the measured tensile strength compared with the ones measured for untreated samples. The tensile strength measured for untreated Teflon is lower than the one for untreated Kapton, in accordance with their WCA values. For immediate metallization of Kapton, the adhesion of the seed layer is increased by factor 3 by the plasma treatment, as it could be expected from the observed WCA decrease. When the ageing time is about few days, the tensile strength is slightly lower but still high compared to the untreated sample. The oxygen plasma exposure of Kapton provides quite stable surface modifications (if conserved

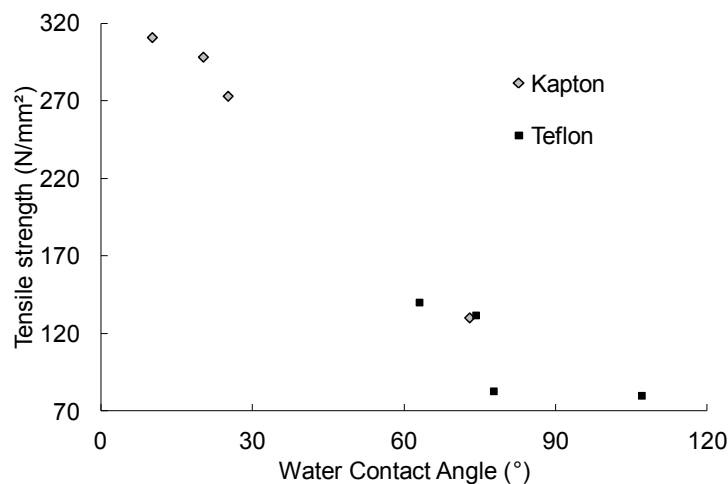
under vacuum) which allows ageing times of several days without a critical loss of adhesion. For metallization of Teflon after an ageing time of 3 hours, the adhesion of the seed layer is increased by factor 2 compared with the untreated film. Note that the tensile strength in this case is comparable with the one measured for the untreated Kapton sample. These observations are coherent with the WCA measurements. When the metallization is done 1 day after the treatment, the tensile strength shows only a small decrease. However, after 5 days, it becomes comparable to the value without any treatment. The plasma exposure of Teflon allows a significant improvement of the polymer/metal adhesion only for short ageing times about several hours (eventually a day). As the tensile strength and thus the adhesion is lower for Teflon (even with the plasma treatment) than Kapton substrates, it becomes crucial for a reliable fabrication process to limit the evolution of the surface modifications by keeping as short as possible the ageing time between the treatment and the metallization.

Figure 11. Evolution of tensile strength of the metallic seed layer deposited on untreated and treated Kapton (a) and FEP Teflon (b) films, with time.



A good correlation can be obtained between the measured tensile strength and the WCA values for Kapton and Teflon surfaces as shown in Figure 12.

Figure 12. Correlation between the measured tensile strength and WCA values for Kapton and Teflon substrates.



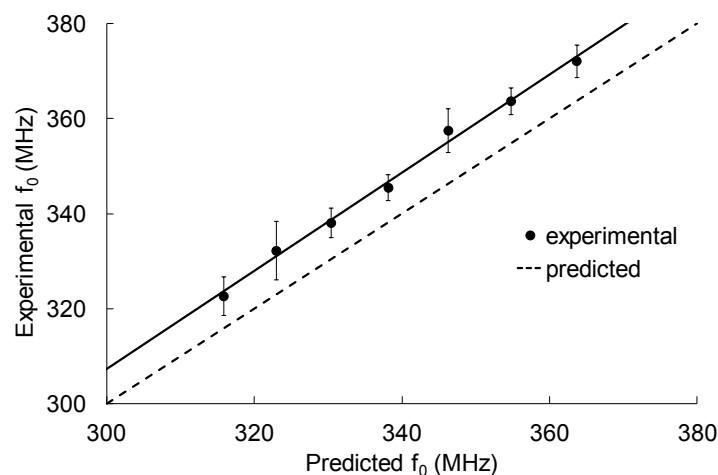
3.3. Fabrication and Characterization of Microantennae on Polymer Substrates

The flexible microantennae fabricated on plasma treated FEP Teflon substrates using copper micromoulding process are shown in Figure 13. The characteristics f_0 and Q of the antennas are measured after fabrication without any packaging. The measured f_0 values are in good agreement with the predicted ones using the analytical model described in [29] (Figure 14), with a standard deviation of 3%, from the model. The measured Q values range from 100 to 120, which are excellent, as expected from the low loss tangent of the Teflon substrate.

Figure 13. Flexible microantennae fabricated on plasma treated FEP Teflon substrates.



Figure 14. Experimental resonant frequencies *versus* predicted ones.



3.4. Optimization of the PDMS Packaging

To ensure biocompatibility of the antennas and to keep the same characteristics independently from the environment, they are coated with PDMS. To investigate the impact of the thickness of this coating both in air and in a conducting environment (saline agar gel phantom simulating the tissues), the PDMS thickness is progressively increased with a path of 20 μm , with thickness ranging from 30 to 400 μm . For each increment, measurements of f_0 and Q are systematically performed in air and in the gel phantom. Preliminary results have shown that the f_0 value in air decreases with the thickness coating, as expected from the PDMS permittivity value (Figure 15). This decrease of f_0 is not linear and more important after deposition of 30 μm of PDMS, probably because a thin coating is sufficient

to confine the most part of the electric field lines. When the electric field lines are totally confined (*i.e.*, thickness about 270 μm), the variation of f_0 in air becomes negligible. In the phantom, with the minimal PDMS thickness (30 μm), f_0 is only half of its value in air. Indeed, a dielectric coupling with the conducting material above the antenna occurs and shifts down the f_0 value. The dielectric coupling decreases with the distance between the top windings and the surface of the antenna, *i.e.*, the packaging thickness. This observation is in agreement with the observation of Bilgen *et al.* [4]. As for measurements in air, the first PDMS layers have a higher impact on the f_0 variation. Finally, the two curves converge to the same value, *i.e.*, 300 MHz, for the same thickness (about 270 μm). For higher PDMS thickness values, f_0 becomes independent from the packaging thickness and from the environment conductivity. Similar behavior was observed by Volland *et al.* with thicknesses of several millimeters on macroscopic antennas [30]. Through the knowledge of the maximal f_0 shift with coating, it is possible to predict the required value just after fabrication to reach the same f_0 value in air and in a conducting environment. Our results clearly indicate that a PDMS thickness higher than 270 μm is suitable to ensure the achievement of the frequency specification for 7 Tesla MRI.

Figure 15. Variation of f_0 with PDMS thickness in air and in the gel phantom.

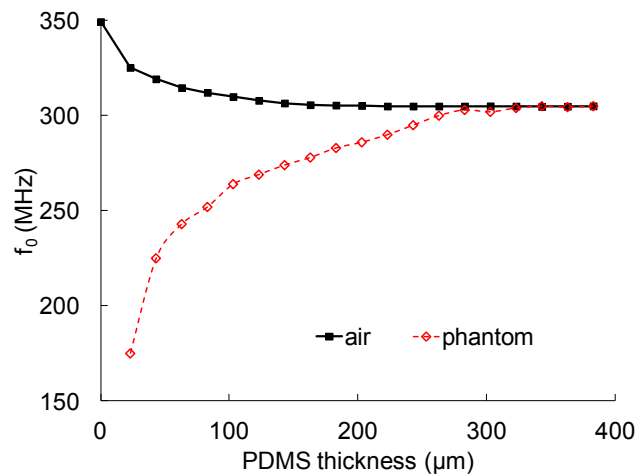
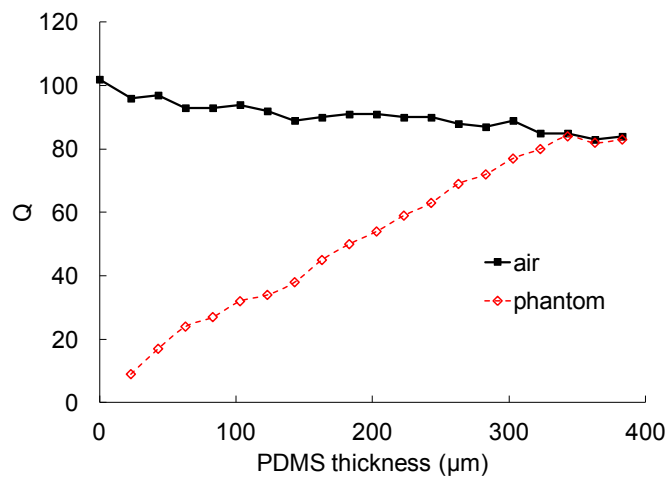


Figure 16. Variation of Q with PDMS thickness in air and in the gel phantom.



The Q value in air decreases with the PDMS thickness, in agreement with the variation of f_0 (Figure 16). In the phantom, when the coating is very thin (30 μm), the Q value is reduced by a factor of 10 compared with the one in air. A similar observation was made by Yung *et al.* [3]. It may be explained by the same reasons as for f_0 . The Q value in the phantom quickly increases with the PDMS thickness until the same final value (about 80) as in air, for thicknesses higher than 350 μm . In these conditions, the Q value is totally suitable to obtain high quality images.

3.5. In Vivo Magnetic Resonance Imaging

After the optimization of the PDMS packaging and successful tests in the gel phantom, we decided to perform *in vivo* imaging of the rat brain. A microantenna with a thick PDMS packaging (about of 300 μm on each side) is implanted at the level of the interhemispheric cleft. An *in vivo* image of the rat brain obtained at 7 Tesla with this implanted microantenna is displayed Figure 17. A 3D FLASH acquisition sequence is used with an in-plane field of view of $2.56 \times 1.92 \text{ cm}^2$ and a matrix of 192×92 . The corresponding in-plane resolution is $100 \times 100 \mu\text{m}^2$. The entire data set is composed of 64 images (slice thickness of 200 μm) corresponding to an explored volume of $2.56 \times 1.92 \times 1.28 \text{ cm}^3$ that covers the entire rat brain. The echo time and repetition time are 11 ms and 50 ms, respectively. The total acquisition time is about 40 min.

Figure 17. *In vivo* image of the rat brain acquired at 7 Tesla from an implanted microantenna with an optimized (300 μm -thick) PDMS packaging.



The brain image reveals a quite large (about 6 mm in diameter) observable volume with sufficiently high SNR. An average SNR of 80 is measured close to the microantenna. The high spatial resolution achieved in all directions allows the visualization of very fine cerebral structures. The realization of this image with a good SNR value constitutes an experimental validation of our miniaturization and PDMS packaging approaches.

4. Conclusions

Polymer thin films have interesting mechanical (flexibility), dielectric (permittivity and loss tangent) and interfacial (biocompatibility) properties which make them suitable both as substrate and as packaging material for implantable MRI microantennae. Dielectric properties of polymer substrates provide a solution to overcome the miniaturization limit, by the use of a monolithic and wireless design based on transmission lines between two conductor windings on both sides of a dielectric material (MTLR design). To benefit from this advantage, specific plasma treatments must be applied to improve the polymer/metal adhesion. We have evidenced the efficiency of O₂ and N₂/H₂ plasma exposure (respectively for Kapton and Teflon films) for this purpose. In the case of Teflon, the ageing time between the surface treatment and the metal deposition is crucial to ensure a reliable adhesion. Good correlation between the wettability (WCA) of the surface and the adhesion (tensile strength) has been established. Additional characterization of the treated surfaces by XPS and AFM techniques should provide a more complete understanding of the induced surface modifications and the observed correlation.

Dielectric properties of polymers offer a solution to the f_0 shift down and the Q degradation induced by the coupling effect in a conducting environment. With PDMS as packaging material, thickness has been optimized in air and in gel phantoms modeling the tissues to obtain characteristics independent from the electrical properties of the surrounding environment. The minimal thickness to achieve this condition is about 300 μm . *In vivo* MR images of the rat brain have been easily obtained at 7 Tesla from an implanted antenna with this packaging thickness. The spatial resolution is $100 \times 100 \times 200 \mu\text{m}^3$ and the SNR is about 80, demonstrating the capability of the system for this application.

We aim to continue to reduce as much as possible the invasiveness of the implantation. The geometric parameters of the antenna are very large compared with the extreme resolution of microfabrication technologies and thus can be still reduced without process concerns. Furthermore, the packaging thickness can be also reduced by the use of other biocompatible materials with higher permittivity than the PDMS one. Surface modifications by plasma treatments could be applied to the packaging material in order to graft appropriate molecules on its surface and so to increase biocompatibility for long-term monitoring. Moreover, a rounded shape for the substrate around the coil that is both adequate to implantation and ergonomic for the surgeon is currently in development.

Acknowledgments

This work is supported by the European project ISEULT, in the Neurospin platform of CEA Saclay. The authors would like to thank Sylvain Massey for contributing in the plasma treatments during his post doctoral position in the Laboratoire du Génie des Procédés Plasmas et Traitements de Surface (LGPPTS, Chimie ParisTech) and Boucif Djemaï from the Institute of Biomedical Imaging (I2BM, Neurospin, CEA Saclay) for the surgical implantation of the antennas into the rat brain. A special thanks is also addressed to the staff of the University Technology Center (CTU) for technical expertise and cleanroom facilities.

References

1. Polikov, V.S.; Tresco, P.A.; Reichert, W.M. Response of brain tissue to chronically implanted neural electrodes. *J. Neurosci. Methods* **2005**, *148*, 1–18.
2. Martin, P.J.; Plewes, D.B.; Henkelman, R.M. MR imaging of blood vessels with an intravascular coil. *J. Mag. Res. Imag.* **1992**, *2*, 421–429.
3. Yung, A.C.; Kolowski, P. Signal-to-noise ratio comparison of phased-array vs. implantable coil for rat spinal cord MRI. *Magn. Reson. Imaging* **2007**, *25*, 1215–1221.
4. Bilgen, M. Magnetic resonance microscopy of spinal cord injury in mouse using a miniaturized implantable RF coil. *J. Neurosci. Methods* **2007**, *159*, 93–97.
5. Serfaty, S.; Haziza, N.; Darrasse, L.; Kan, S. Multi-turn split-conductor transmission-line resonators. *Magnet. Reson. Med.* **1997**, *38*, 687–689.
6. Renaud, L.; Armenean, M.; Berry, L.; Kleimann, P.; Morin, P.; Pitaval, M.; O'Brien, J.; Brunet, M.; Saint-Jalmes, H. Implantable planar RF microcoils for NMR microspectroscopy. *Sens. Actuat. A* **2002**, *99*, 244–248.
7. Coutrot, A.-L.; Dufour-Gergam, E.; Quemper, J.-M.; Martincic, E.; Gilles, J.-P.; Grandchamp, J.P.; Matlosz, M.; Sanchez, A.; Darrasse, L.; Ginefri, J.-C. Copper micromolding process for NMR microinductors realization. *Sens. Actuat. A* **2002**, *99*, 49–54.
8. Uelzen, T.; Fandray, S.; Müller, J. Mechanical and electrical properties of electroplated copper for MR-imaging coils. *Microsyst. Technol.* **2006**, *12*, 343–351.
9. Eilersiek, D.; Harms, S.; Casanova, F.; Blümich, B.; Mokwa, W.; Schnakenberg, U. Flexible RF microcoils with integrated capacitor for NMR applications. In *Proceedings of MicroMechanics Europe (MME'05)*, Göteborg, Sweden, 4–6 September 2005; pp. 256–259.
10. Zhang, X.; Ugurbil, K.; Chen, W. Microstrip RF surface coil design for extremely high-field MRI and spectroscopy. *Magnet. Reson. Med.* **2001**, *46*, 443–450.
11. Eroglu, S.; Gimi, B.; Roman, B.; Friedman, G.; Magin, R.L. NMR spiral surface microcoils: design, fabrication and imaging. *Concept Magnetic Res.* **2003**, *17B*, 1–10.
12. Woytasik, M.; Ginefri, J.-C.; Raynaud, J.-S.; Poirier-Quinot, M.; Dufour-Gergam, E.; Grand-champ, J.-P.; Robert, P.; Gilles, J.-P.; Martincic, E.; Girard, O.; Darrasse, L. Characterization of flexible RF microcoils dedicated to local MRI. *Microsyst. Technol.* **2007**, *13*, 1575–1580.
13. Ahmad, M.M.; Syms, R.R.A.; Young, I.R.; Mathew, B.; Casperz, W.; Taylor-Robinson, S.D.; Wadsworth, C.A.; Gedroyc, W.M.W. Catheter-based flexible microcoil RF detectors for internal magnetic resonance imaging. *J. Micromech. Microeng.* **2009**, *20*, 074011.
14. Eilersiek, D.; Fassbender, H.; Bruners, P.; Pfeiffer, J.G.; Penzkofer, T.; Mahnken, A.H.; Schmitz-Rode, T.; Mokwa, W.; Schnakenberg, U. A monolithically fabricated flexible resonant circuit for catheter tracking in magnetic resonance imaging. *Sens. Actuat. B* **2009**, *144*, 432–436.
15. Syms, R.R.A.; Young, I.R.; Ahmad, M.M.; Rea, M.; Wadsworth, C.A.; Taylor-Robinson, S.-D. Thin-film detector system for internal magnetic resonance imaging. *Sens. Actuat. A* **2010**, *163*, 15–24.
16. Mata, A.; Fleischman, A.J.; Roy, S. Characterization of Polydimethylsiloxane (PDMS) properties for biomedical micro/nanosystems. *Biomed. Microdev.* **2005**, *7*, 281–293.

17. Egitto, F.D.; Matienzo, L.J. Plasma modification of polymer surfaces for adhesion improvement. *IBM J. Res. Develop.* **1994**, *38*, 423–439.
18. Brewis, D.M.; Dahm, R.H. *Adhesion to Fluoropolymers*, Rapra Technology Limited: Shrewsbury, UK, 2006; Volume 16, pp. 17–23.
19. Sarra-Bournet, C.; Ayotte, G.; Turgeon, S.; Massines, F.; Laroche, G. Effects of chemical composition and the addition of H₂ in a N₂ atmospheric pressure dielectric barrier discharge on polymer surface functionalization. *Langmuir* **2009**, *25*, 9432–9440.
20. Woytasik, M.; Grandchamp, J.-P.; Dufour-Gerfame, E.; Gilles, J.-P.; Megherbi, S.; Martincic, E.; Mathias, H.; Crozat, P. Two-dimensional microcoil fabrication process for three-axis magnetic sensors on flexible substrates. *Sens. Actuat. A* **2006**, *132*, 2–7.
21. Tatoulian, M.; Shahidzadeh, N.; Arefi-Khonsari, F.; Amouroux, J. Comparison of the efficiency of N₂ and NH₃ plasma treatments to improve the adhesion of PP films to in-situ deposited Aluminium coatings. Study of ageing phenomena in terms of acid-base properties. *Int. J. Adhesion Adhesives* **1995**, *15*, 177–184.
22. Neubauer, E.; Korb, G.; Eisenmenger-Sittner, C.; Bangert, H.; Chotikaprakahn, S.; Dietzel, D.; Mansanares, A.M.; Bein, B.K. The influence of mechanical adhesion of copper coatings on carbon surfaces on the interfacial thermal contact resistance. *Thin Solid Films* **2003**, *433*, 160–165.
23. Jeon, B.J.; Lee, S.; Lee, J.K. Adhesion characteristics of copper thin films deposited on PET substrate by electron cyclotron resonance-metal organic chemical vapor deposition. *Surf. Coat. Tech.* **2008**, *202*, 1839–1846.
24. Ginefri, J.-C.; Durand, E.; Darrasse, L. Quick measurement of nuclear magnetic resonance coil sensitivity with a single-loop probe. *Rev. Sci. Instrum.* **1999**, *70*, 4730–4731.
25. Darrasse, L.; Kassab, G. Quick measurement of NMR-coil sensitivity with a dual-loop probe. *Rev. Sci. Instrum.* **1993**, *64*, 1841–1844.
26. Chen, Q. Investigation of corona charge stability mechanisms in polytetrafluoroethylene (PTFE) teflon films after plasma treatment. *J. Electrostat.* **2003**, *59*, 3–13.
27. Tatoulian, M.; Arefi-Khonsari, F.; Mabilite-Rouger, I.; Amouroux, J.; Gheorgiu, M.; Bouchier, D. Role of helium plasma pre-treatment in the stability of the wettability, adhesion and mechanical properties of ammonia plasma-treated polymers: Application to the Al-polypropylene system. *J. Adhesion Sci. Technol.* **1995**, *9*, 923–934.
28. Morra, M.; Occhiello, E.; Garbassi, F. Dynamics of Plasma Treated Polymer Surfaces: Mechanisms and Effects. In *Proceedings of the 1st International Conference of Polymer Solid Interfaces*, Namur, Belgium, 2–6 September 1991; pp. 407–428.
29. Megherbi, S.; Ginefri, J.-C.; Darrasse, L.; Raynaud, G.; Pône, J.-F.; Behavioral Vhdl-Ams model and experimental validation of a Nuclear Magnetic Resonance sensor. *Microsyst. Technol.* **2005**, *12*, 38–43.
30. Volland, N.A.; Mareci, T.H.; Constantinidis, I.; Simpson, N.E. Development of an inductively coupled MR coil system for imaging and spectroscopic analysis of an implantable bioartificial construct at 11.1T. *Magnet. Reson. Med.* **2010**, *63*, 998–1006.